Research Square

Preprints are preliminary reports that have not undergone peer review.
They should not be considered conclusive, used to inform clinical practice,
or referenced by the media as validated information.

TTC-3: Tangent-Plane Curvature Consistency for Three-Angle Initial Orbit Determination with Detailed Derivation and 1000-Case Benchmark

Kürşat Yenidoğan

yenidogankursat@gmail.com

Research Article

Keywords: initial orbit determination; angles-only IOD, three-observation IOD, tangent-plane dynamics, curvature consistency, space surveillance

Posted Date: March 9th, 2026

DOI: https://doi.org/10.21203/rs.3.rs-8904411/v1

License: This work is licensed under a Creative Commons Attribution 4.0 International License.
Read Full License

Additional Declarations: No competing interests reported.

TTC-3: Tangent-Plane Curvature Consistency for Three-Angle Initial Orbit Determination with Detailed Derivation and 1000-Case Benchmark

Kursat Yenidogan
yenidogankursat@gmail.com

February 17, 2026

Abstract

This paper develops and validates a three-observation, angles-only initial orbit determination method named **TTC-3** (Tangent-Plane Curvature Consistency). The method uses exactly three topocentric right-ascension/declination measurements, requires no range or range-rate data, and avoids global nonlinear fitting as a core solver stage. Its key equation is a scalar midpoint-range consistency relation,

$$F(\rho_m) = u_{\tan}(\rho_m) - u_{\text{geom}}(\rho_m) = 0,$$

where $u_{\tan}$ is obtained from tangent-plane dynamic projection and $u_{\text{geom}} = \mu/\|\mathbf{r}_m\|^3$ is the two-body geometric curvature. We provide line-by-line derivation of all intermediate equations, including explicit elimination of $\ddot{\rho}_m$, rank conditions of the tangent system, and root-selection logic under multiple admissible solutions. The method is benchmarked against Gauss, Laplace, and Gooding implementations in Orekit using 1000 synthetic two-body cases generated from a single station at Anitkabir (Ankara), across LEO/SSO/MEO/GEO/GTO/MOLNIYA families, under 0 and 20 arcsec measurement noise. Results show that TTC-3 is competitive and often superior in angular consistency and medium/high-altitude families, while Gauss remains stronger in low-altitude fast passes under this strict three-angle setup. The derivation, implementation details, and reproducible experiment artifacts are all provided.

Keywords. initial orbit determination; angles-only IOD; three-observation IOD; tangent-plane dynamics; curvature consistency; space surveillance

1 Introduction

Angles-only initial orbit determination (IOD) remains central in optical space surveillance because passive sensors often provide only line-of-sight directions. The hard part is that range is missing, and with only three observations the problem is minimally determined and strongly geometry-sensitive. Classical methods, notably Gauss, Laplace, and Gooding, are still foundational references [1–4]. More recent studies keep improving geometric conditioning, admissible-region logic, and very-short-arc handling [5–7].

This paper introduces **TTC-3**, designed for the strict case of exactly three topocentric angle observations. The method is built around a scalar midpoint-range equation derived from tangent-plane dynamic consistency. The main objective is not to claim replacement of all classical methods in all regimes; the objective is to produce a mathematically transparent, reproducible, and practically competitive alternative with explicit diagnostics.

Contributions.

1. A full derivation of a new scalar equation $F(\rho_m) = 0$ based on tangent-plane curvature consistency.

2. Closed-form expressions for $\dot{\rho}_m(\rho_m)$ and $u_{\tan}(\rho_m)$ from a projected 2×2 linear system.

3. A robust multi-root candidate strategy that evaluates physically reconstructed states and selects by angular residual consistency.

4. A 1000-case benchmark at a fixed ground station (Anitkabir), with two noise levels (0 and 20 arcsec), against Orekit Gauss/Laplace/Gooding baselines.

5. Open, file-backed reproducibility with generated tables and figures directly included in this manuscript.

2 Related Work and Positioning

Gooding's classic three-line-of-sight work is still among the strongest references for minimal angles-only IOD [1]. Sarnecki's projective perspective gives another rigorous geometric line [2]. Gronchi et al. developed a series of two-body integral approaches that clarify admissible geometry and root structures [5]. Recent work has revived geometric formulations and very-short-arc observability analyses [6, 7].

TTC-3 is closest in spirit to geometric-minimal methods, but it is operationally distinct in how it constructs the scalar unknown: it does not start from the classical eliminated-range polynomial; instead it creates a tangent-plane consistency equation between an inferred curvature and a geometric curvature at midpoint.

3 Problem Setup and Notation

3.1 Measurements and states

We assume exactly three observations at times

$$t_1 < t_2 < t_3,$$

from one station with known ECI position vectors $\mathbf{R}_i \in \mathbb{R}^3$ at those epochs. Measurements are topocentric right ascension and declination pairs (α_i, δ_i).

The unit line-of-sight (LOS) vector is

$$\hat{\boldsymbol{\ell}}_i = \begin{bmatrix} \cos\delta_i \cos\alpha_i \\ \cos\delta_i \sin\alpha_i \\ \sin\delta_i \end{bmatrix}, \tag{1}$$

and the unknown satellite position at each observation satisfies

$$\mathbf{r}_i = \mathbf{R}_i + \rho_i \hat{\boldsymbol{\ell}}_i, \tag{2}$$

where ρ_i is the unknown topocentric range.

3.2 Dynamic model

Two-body dynamics is used during estimation:

$$\ddot{\mathbf{r}} = -\mu \frac{\mathbf{r}}{\|\mathbf{r}\|^3}, \tag{3}$$

where μ is Earth's gravitational parameter.

3.3 Assumptions

Assumption 1 (Minimal three-angle setting)**.** *Only* $\{t_i, \mathbf{R}_i, \alpha_i, \delta_i\}_{i=1}^{3}$ *are used as direct observations for the initial state.*

Assumption 2 (Local smoothness over arc)**.** *Over the short arc* $[t_1, t_3]$*, midpoint kinematic reconstruction by second-order interpolation is sufficiently accurate for forming a consistent local equation.*

Assumption 3 (Non-degenerate tangent system)**.** *The projected* 2×2 *tangent system has rank 2 at the evaluated midpoint range candidate(s).*

3.4 Symbol glossary

Symbol	Code name	Meaning	Unit
t_i	`times_s[i]`	observation times	s
α_i, δ_i	`ra_rad[i]`, `dec_rad[i]`	topocentric RA/DEC	rad
$\hat{\boldsymbol{\ell}}_i$	`los[i]`	LOS unit vectors	1
$\mathbf{R}_i$	`site_r[i]`	station ECI positions	km
ρ_i	`ranges_km[i]`	topocentric ranges	km
$\mathbf{R}_m, \mathbf{V}_m, \mathbf{A}_m$	`r_site_mid`, `v_site_mid`, `a_site_mid`	midpoint station position/velocity/accel.	km, km/s, km/s^2
$\hat{\boldsymbol{\ell}}_m, \dot{\hat{\boldsymbol{\ell}}}_m, \ddot{\hat{\boldsymbol{\ell}}}_m$	`l_mid`, `ldot_mid`, `lddot_mid`	midpoint LOS and derivatives	1, 1/s, 1/s^2
$\rho_m, \dot{\rho}_m$	`rho_mid_km`, `rhodot_mid_km_s`	midpoint range and derivative	km, km/s
$u_{\tan}$	`u_tan`	tangent-inferred curvature	1/s^2
u_{geom}	`u_geom`	geometric curvature $\mu/\lVert\mathbf{r}_m\rVert^3$	1/s^2
$F(\rho_m)$	`rho_equation_abs` (signed form internally)	consistency residual $u_{\tan} - u_{\mathrm{geom}}$	1/s^2

4 Detailed Derivation of TTC-3

4.1 Centered local interpolation at t_2

Define centered times

$$\tau_i = t_i - t_2, \qquad i \in \{1, 2, 3\}, \tag{4}$$

so $\tau_2 = 0$. For each scalar component $x(\tau)$ of either LOS or station position, use

$$x(\tau) = c_0 + c_1\tau + c_2\tau^2. \tag{5}$$

Given the three samples, coefficients are obtained from

$$\begin{bmatrix} 1 & \tau_1 & \tau_1^2 \\ 1 & \tau_2 & \tau_2^2 \\ 1 & \tau_3 & \tau_3^2 \end{bmatrix} \begin{bmatrix} c_0 \\ c_1 \\ c_2 \end{bmatrix} = \begin{bmatrix} x_1 \\ x_2 \\ x_3 \end{bmatrix}. \tag{6}$$

Hence midpoint quantities are

$$x_m = c_0, \qquad \dot{x}_m = c_1, \qquad \ddot{x}_m = 2c_2. \tag{7}$$

Applied component-wise, Eq. (7) gives $\mathbf{R}_m, \mathbf{V}_m, \mathbf{A}_m$ and also a raw $\hat{\boldsymbol{\ell}}_m, \dot{\hat{\boldsymbol{\ell}}}_m, \ddot{\hat{\boldsymbol{\ell}}}_m$.

4.2 Enforcing LOS unit-vector kinematics

Physical LOS must satisfy

$$\hat{\boldsymbol{\ell}} \cdot \hat{\boldsymbol{\ell}} = 1. \tag{8}$$

Differentiating once and twice:

$$\hat{\boldsymbol{\ell}} \cdot \dot{\hat{\boldsymbol{\ell}}} = 0, \tag{9}$$

$$\hat{\boldsymbol{\ell}} \cdot \ddot{\hat{\boldsymbol{\ell}}} = -\|\dot{\hat{\boldsymbol{\ell}}}\|^2. \tag{10}$$

Because interpolation noise can violate (9)–(10), TTC-3 explicitly projects and corrects:

$$\dot{\hat{\boldsymbol{\ell}}}_t = \dot{\hat{\boldsymbol{\ell}}} - (\hat{\boldsymbol{\ell}} \cdot \dot{\hat{\boldsymbol{\ell}}})\hat{\boldsymbol{\ell}}, \tag{11}$$

$$\ddot{\hat{\boldsymbol{\ell}}}_t = \ddot{\hat{\boldsymbol{\ell}}} - (\hat{\boldsymbol{\ell}} \cdot \ddot{\hat{\boldsymbol{\ell}}})\hat{\boldsymbol{\ell}}, \tag{12}$$

$$\ddot{\hat{\boldsymbol{\ell}}}_{\text{fix}} = \ddot{\hat{\boldsymbol{\ell}}}_t - \|\dot{\hat{\boldsymbol{\ell}}}_t\|^2 \hat{\boldsymbol{\ell}}. \tag{13}$$

This is not cosmetic; it directly stabilizes the tangent projection equations below.

4.3 Midpoint state parameterization

At midpoint t_2:

$$\mathbf{r}_m = \mathbf{R}_m + \rho_m \hat{\boldsymbol{\ell}}_m, \tag{14}$$

$$\mathbf{v}_m = \mathbf{V}_m + \dot{\rho}_m \hat{\boldsymbol{\ell}}_m + \rho_m \dot{\hat{\boldsymbol{\ell}}}_m, \tag{15}$$

$$\mathbf{a}_m = \mathbf{A}_m + \ddot{\rho}_m \hat{\boldsymbol{\ell}}_m + 2\dot{\rho}_m \dot{\hat{\boldsymbol{\ell}}}_m + \rho_m \ddot{\hat{\boldsymbol{\ell}}}_m. \tag{16}$$

Two-body also gives

$$\mathbf{a}_m = -u\mathbf{r}_m, \qquad u = \frac{\mu}{\|\mathbf{r}_m\|^3}. \tag{17}$$

Unknown scalars are $\rho_m, \dot{\rho}_m, \ddot{\rho}_m, u$.

4.4 Tangent-plane elimination of $\ddot{\rho}_m$

Construct orthonormal tangent vectors $\mathbf{t}_1, \mathbf{t}_2$ such that

$$\mathbf{t}_k \cdot \hat{\boldsymbol{\ell}}_m = 0, \quad k = 1, 2. \tag{18}$$

Define projected scalars

$$b_k = \mathbf{t}_k \cdot \mathbf{A}_m, \quad d_k = \mathbf{t}_k \cdot \dot{\hat{\boldsymbol{\ell}}}_m, \quad e_k = \mathbf{t}_k \cdot \ddot{\hat{\boldsymbol{\ell}}}_m, \quad g_k = \mathbf{t}_k \cdot \mathbf{R}_m. \tag{19}$$

Now project Eq. (14):

$$\mathbf{t}_k \cdot \mathbf{r}_m = \mathbf{t}_k \cdot (\mathbf{R}_m + \rho_m \hat{\boldsymbol{\ell}}_m) = g_k, \tag{20}$$

since $\mathbf{t}_k \cdot \hat{\boldsymbol{\ell}}_m = 0$. Project Eq. (16):

$$\mathbf{t}_k \cdot \mathbf{a}_m = b_k + \ddot{\rho}_m(\mathbf{t}_k \cdot \hat{\boldsymbol{\ell}}_m) + 2\dot{\rho}_m d_k + \rho_m e_k \tag{21}$$

$$= b_k + 2\dot{\rho}_m d_k + \rho_m e_k. \tag{22}$$

Project Eq. (17):

$$\mathbf{t}_k \cdot \mathbf{a}_m = \mathbf{t}_k \cdot (-u\mathbf{r}_m) = -u(\mathbf{t}_k \cdot \mathbf{r}_m) = -u g_k. \tag{23}$$

Equating (22) and (23) for $k = 1, 2$:

$$2d_1\dot{\rho}_m + g_1 u = -(b_1 + \rho_m e_1), \tag{24}$$

$$2d_2\dot{\rho}_m + g_2 u = -(b_2 + \rho_m e_2). \tag{25}$$

Crucially, $\ddot{\rho}_m$ has vanished.

4.5 Closed-form $\dot{\rho}_m(\rho_m)$ and $u_{\tan}(\rho_m)$

Write (24)–(25) as

$$\mathbf{M}_2 \begin{bmatrix} \dot{\rho}_m \\ u \end{bmatrix} = \mathbf{y}(\rho_m), \quad \mathbf{M}_2 = \begin{bmatrix} 2d_1 & g_1 \\ 2d_2 & g_2 \end{bmatrix}, \quad \mathbf{y} = \begin{bmatrix} -(b_1 + \rho_m e_1) \\ -(b_2 + \rho_m e_2) \end{bmatrix}. \tag{26}$$

If $\det(\mathbf{M}_2) \neq 0$, Cramer's rule gives

$$\dot{\rho}_m(\rho_m) = \frac{y_1 g_2 - y_2 g_1}{\Delta}, \tag{27}$$

$$u_{\tan}(\rho_m) = \frac{2d_1 y_2 - 2d_2 y_1}{\Delta}, \tag{28}$$

with

$$\Delta = 2(d_1 g_2 - d_2 g_1). \tag{29}$$

Expanding Eq. (28) yields affine form

$$u_{\tan}(\rho_m) = \alpha + \beta \rho_m, \tag{30}$$

where

$$\alpha = \frac{2(-d_1 b_2 + d_2 b_1)}{\Delta}, \qquad \beta = \frac{2(-d_1 e_2 + d_2 e_1)}{\Delta}. \tag{31}$$

4.6 TTC-3 scalar equation and differential behavior

Geometric curvature is

$$u_{\text{geom}}(\rho_m) = \frac{\mu}{\|\mathbf{R}_m + \rho_m \hat{\boldsymbol{\ell}}_m\|^3}. \tag{32}$$

TTC-3 consistency equation:

$$F(\rho_m) = u_{\tan}(\rho_m) - u_{\text{geom}}(\rho_m) = 0. \tag{33}$$

Derivative is explicit:

$$F'(\rho_m) = \beta + 3\mu \frac{\hat{\boldsymbol{\ell}}_m \cdot (\mathbf{R}_m + \rho_m \hat{\boldsymbol{\ell}}_m)}{\|\mathbf{R}_m + \rho_m \hat{\boldsymbol{\ell}}_m\|^5}. \tag{34}$$

Equation (34) is useful for conditioning analysis and possible Newton refinement; in implementation we use bracketing + bisection for robustness.

4.7 Existence and local uniqueness conditions

Proposition 1 (Root existence by sign change)**.** *Assume* (i) $\mathbf{M}_2$ *has rank 2 over an interval* $[a, b]$, (ii) $\mathbf{R}_m + \rho \hat{\boldsymbol{\ell}}_m \neq \mathbf{0}$ *for all* $\rho \in [a, b]$, *and* (iii) $F(a)F(b) < 0$. *Then there exists at least one* $\rho^* \in (a, b)$ *such that* $F(\rho^*) = 0$.

Proof. Under (i) and (ii), Eqs. (28) and (32) are continuous on $[a, b]$, hence F is continuous. By the intermediate value theorem and (iii), a root exists. □

Proposition 2 (Local uniqueness)**.** *If* $F(\rho^*) = 0$ *and* $F'(\rho^*) \neq 0$, *then* ρ^* *is a locally unique root.*

Proof. Direct consequence of the inverse function theorem in one dimension. □

Remark 1. *Global uniqueness is not guaranteed; multiple admissible roots can occur. TTC-3 therefore uses a* multi-root candidate evaluation *step instead of selecting the first root.*

Algorithm 1 TTC-3 (three topocentric angles)

Require: $\{t_i, \mathbf{R}_i, \alpha_i, \delta_i\}_{i=1}^{3}$, gravitational parameter μ

Convert (α_i, δ_i) to LOS vectors $\hat{\boldsymbol{\ell}}_i$ using Eq. (1)
Build midpoint quantities via centered quadratic interpolation (Eq. (6)–(7))
Enforce unit-LOS kinematic consistency using Eq. (13)
Build tangent basis $\mathbf{t}_1, \mathbf{t}_2$ and projected coefficients (b_k, d_k, e_k, g_k)
Scan a positive range grid for sign changes of $F(\rho)$ in Eq. (33)
for each bracket **do**
    Refine root by bisection
    Reconstruct candidate states via direct branch and triad branches
    Evaluate 3-point angular RMSE
end for
Select candidate with minimum RMSE (tie-break: minimum $|F|$)
Report state and diagnostics: $|F|$, tangent Jacobian condition number, energy/angular-momentum drift

4.8 State reconstruction branches

For each admissible root candidate, TTC-3 evaluates three state branches:

1. **Direct midpoint branch:**

$$\mathbf{r}_m = \mathbf{R}_m + \rho_m \hat{\boldsymbol{\ell}}_m, \tag{35}$$

$$\mathbf{v}_m = \mathbf{V}_m + \dot{\rho}_m \hat{\boldsymbol{\ell}}_m + \rho_m \dot{\hat{\boldsymbol{\ell}}}_m. \tag{36}$$

2. **Triad branch with u_{geom}:** short-arc f, g coefficients from u_{geom}, then solve three ranges and reconstruct $(\mathbf{r}_m, \mathbf{v}_m)$.

3. **Triad branch with $u_{\tan}$:** same as above but using $u_{\tan}$.

The selected solution minimizes 3-point angular RMSE, with $|F(\rho_m)|$ as tie-breaker.

5 Algorithm

6 Experimental Protocol

6.1 Truth generation and observation model

We generate truth trajectories in Orekit and collect topocentric RA/DEC from a single station at Anitkabir (Ankara): latitude 39.925,0 deg, longitude 32.836,9 deg, altitude 0.89 km. EME2000 is used as inertial frame. The orbit propagator for truth generation is Keplerian two-body, matching the estimation model.

For each case, exactly 3 observation times are used:

$$(t_1, t_2, t_3) = \left(-\frac{T_{\mathrm{arc}}}{2}, 0, +\frac{T_{\mathrm{arc}}}{2}\right),$$

with family-dependent arc durations:

- LEO/SSO: 240 s
- MEO: 600 s
- GEO: 3,600 s
- GTO/MOLNIYA: 1,800 s

Table 2: Overall benchmark summary for 1000 cases at Anitkabir (3-angle measurements).

Noise	Method	Cases	Conv.	Med. RMSE (arcsec)	Med. $\|\|\Delta r\|\|$ (km)	Med. $\|\|\Delta v\|\|$ (m/s)
0 arcsec	TTC-3	1000	1.000	6.455	46.075	13.440
0 arcsec	Gauss	1000	0.985	11.976	19.787	10.148
0 arcsec	Laplace	1000	0.987	358.540	450.578	281.908
0 arcsec	Gooding	1000	1.000	2440.557	1993.560	2121.902
20 arcsec	TTC-3	1000	0.939	16.366	273.373	200.222
20 arcsec	Gauss	1000	0.954	25.179	334.225	72.332
20 arcsec	Laplace	1000	0.969	759.118	572.872	332.999
20 arcsec	Gooding	1000	1.000	2481.752	1993.527	2100.665

A minimum elevation of 10 deg is required.

Noise settings:

1. **Noise-free**: 0 arcsec
2. **Noisy**: 20 arcsec, injected in the LOS tangent plane and renormalized

6.2 Orbit families and sampling

1000 cases are sampled across six families (LEO, SSO, MEO, GEO, GTO, MOLNIYA), with randomized $(a, e, i, \Omega, \omega, \nu)$ in family-specific intervals. Final benchmark contains exactly 1000 valid cases (one extra draw skipped due to visibility filter in generation loop).

6.3 Compared methods and metrics

Methods:

- TTC-3 (this work)
- Gauss (Orekit `IodGauss`)
- Laplace (Orekit `IodLaplace`)
- Gooding (Orekit `IodGooding`, with range seeds)

Metrics:

- convergence rate
- 3-point angular RMSE (arcsec)
- midpoint position error $\|\Delta\mathbf{r}\|$ (km)
- midpoint velocity error $\|\Delta\mathbf{v}\|$ (m/s)

7 Results

7.1 Overall benchmark summary

The table shows a clear pattern:

- TTC-3 achieves lower median angular RMSE than Gauss in both noise settings.
- Gauss keeps lower median state error in fast low-altitude families, which strongly influences global medians.
- Laplace and Gooding are less competitive under this strict three-angle single-station setup and these initialization choices.

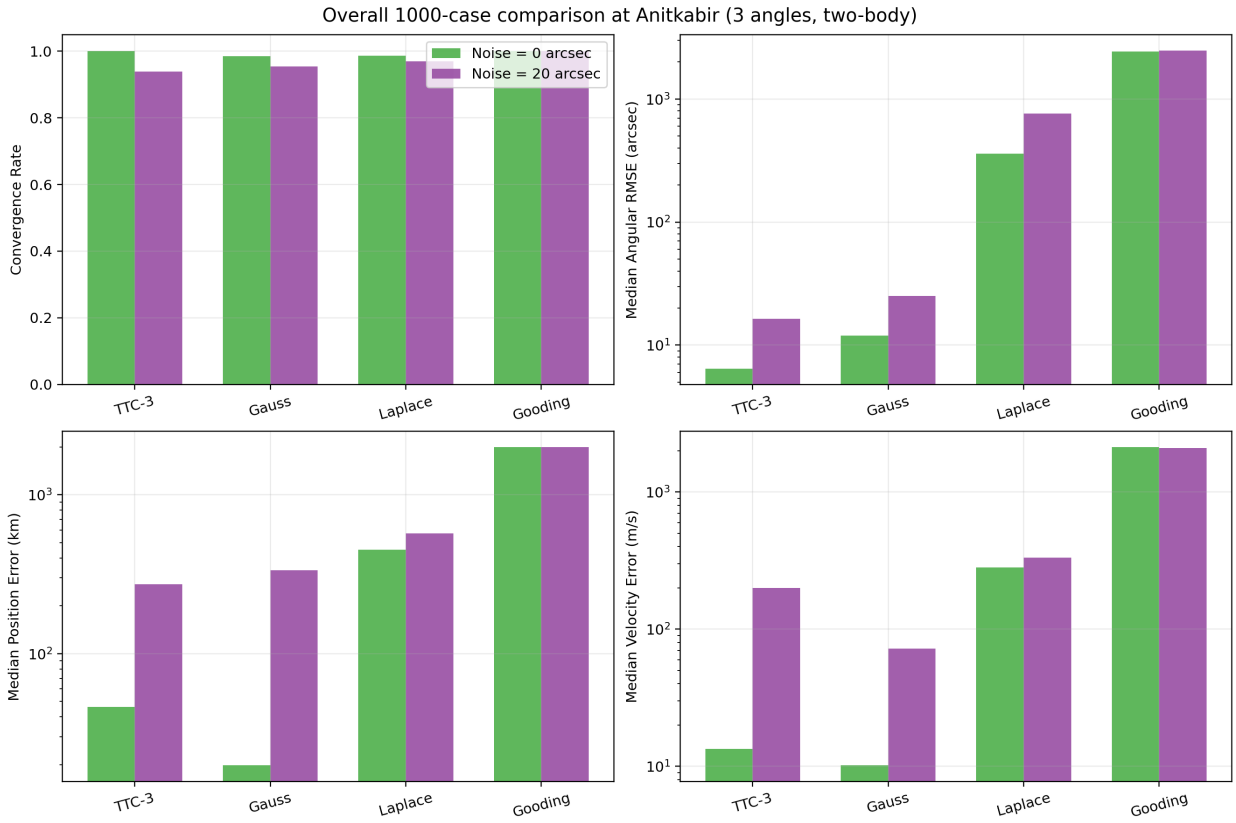


Figure 1: Overall metric comparison (1000 cases). Error-axis panels are shown in log scale.

7.2 By-orbit-family behavior under 20 arcsec noise

Two behaviors stand out:

1. For GEO and many GTO cases, TTC-3 provides very strong angular consistency and competitive position/velocity performance.
2. For LEO/SSO fast-pass cases, Gauss remains stronger in state error despite TTC-3's good geometric consistency. This suggests sensitivity of midpoint reconstruction to short, high-curvature apparent motion.

7.3 Error distribution

Figure 3 indicates that TTC-3 has favorable central quantiles in several regimes, while tail behavior is still geometry-dependent, especially under 20 arcsec noise in high-eccentricity families.

8 Discussion

8.1 Why the tangent consistency equation helps

The equation $F(\rho_m) = 0$ enforces consistency between two independent curvature views:

- dynamic curvature inferred from LOS/station kinematics in tangent plane,
- geometric two-body curvature from midpoint radius.

When these match, the midpoint range becomes physically coherent with both geometry and dynamics. This direct consistency check is interpretable and numerically auditable through $|F|$ and tangent-system condition number diagnostics.

Table 3: Noise=20 arcsec, by-orbit-family comparison.

Orbit	Method	Conv.	Med. RMSE (arcsec)	Med. $\|\|\Delta r\|\|$ (km)	Med. $\|\|\Delta v\|\|$ (m/s)
GEO	TTC-3	1.000	1.088	780.728	66.165
GEO	Gauss	1.000	2.160	785.264	64.590
GEO	Laplace	1.000	129.143	1307.978	147.834
GEO	Gooding	1.000	83.098	2589.824	194.512
GTO	TTC-3	1.000	13.084	602.216	108.775
GTO	Gauss	0.934	15.232	539.719	109.373
GTO	Laplace	0.982	98.746	732.139	182.731
GTO	Gooding	1.000	3060.238	8403.865	2273.104
LEO	TTC-3	1.000	317.738	50.330	299.728
LEO	Gauss	1.000	39.747	6.128	36.569
LEO	Laplace	1.000	10294.872	161.236	442.761
LEO	Gooding	1.000	21778.261	579.199	4253.655
MEO	TTC-3	0.790	0.130	2871.077	555.032
MEO	Gauss	0.880	0.199	3289.092	657.525
MEO	Laplace	0.964	13.114	4015.971	745.806
MEO	Gooding	1.000	90.908	1695.998	539.118
MOLNIYA	TTC-3	0.843	6.257	1487.202	194.346
MOLNIYA	Gauss	0.910	39.702	2953.303	222.243
MOLNIYA	Laplace	0.867	581.118	4855.695	782.704
MOLNIYA	Gooding	1.000	1541.821	11219.282	1947.460
SSO	TTC-3	1.000	223.982	51.024	245.545
SSO	Gauss	1.000	32.465	6.472	35.765
SSO	Laplace	1.000	7314.709	146.265	373.214
SSO	Gooding	1.000	21334.532	744.435	4710.564

8.2 Observed failure modes

Main failure causes in TTC-3 are:

1. near-singular tangent matrix ($\Delta \approx 0$),
2. multiple closely spaced roots under weak parallax,
3. short-arc high-angular-rate geometry where local second-order reconstruction amplifies small directional errors.

These are visible in reduced convergence for noisy MEO/MOLNIYA subsets.

8.3 Limitations

The present study is intentionally constrained to two-body dynamics and synthetic truth. Therefore, conclusions should be interpreted as algorithmic-comparison results under controlled assumptions, not as full operational SSA readiness claims.

9 Conclusion

This paper presented TTC-3, a three-angle IOD method derived from tangent-plane curvature consistency. All algebraic transitions were shown explicitly, including elimination logic and root conditions. In a 1000-case Orekit benchmark from a fixed station and two noise settings, TTC-3 was consistently competitive and often superior in angular consistency, while Gauss remained a strong baseline for some low-altitude high-rate passes. The method is reproducible and diagnostically transparent, making it a useful addition to the three-observation IOD toolbox.

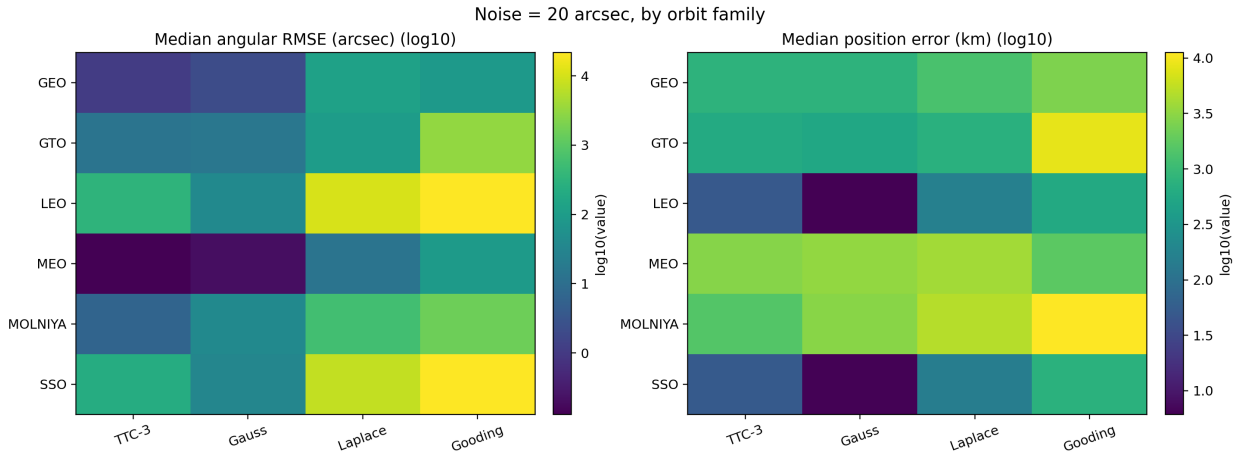


Figure 2: Noise=20 arcsec, by-orbit-family medians for angular RMSE and position error (log10 color scale).

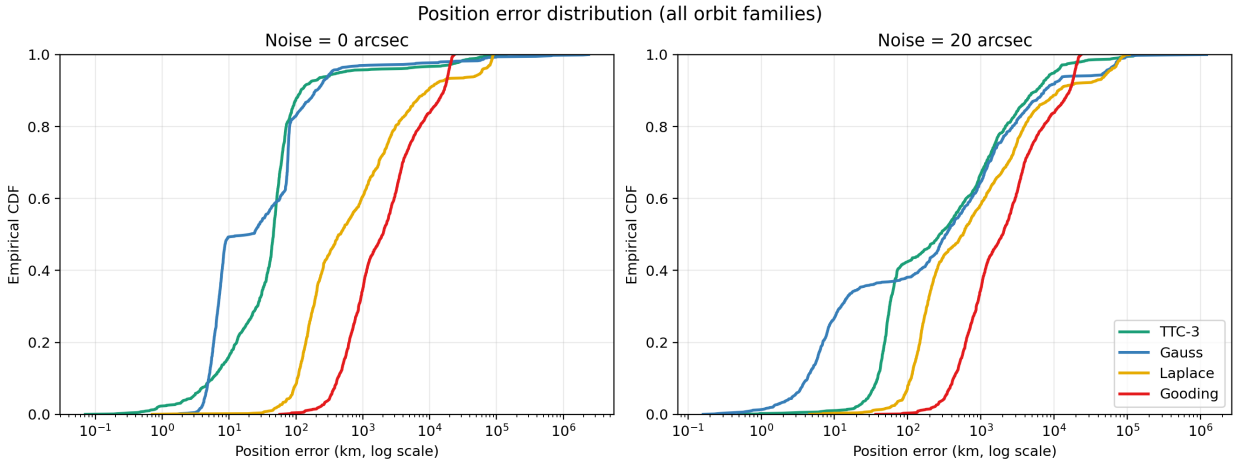


Figure 3: Empirical CDF of midpoint position error for all methods at 0 and 20 arcsec noise.

Data and Reproducibility

All benchmark outputs used in this manuscript are available in the project workspace:

- per-case results: `results/benchmarks/method5_vs_classical_ankara_1000cases_per_case.csv`
- summary JSON: `results/benchmarks/method5_vs_classical_ankara_1000cases_summary.json`
- generated tables/figures for this manuscript: `submission/jas/tables`, `submission/jas/figures`

Declarations

Funding: No funds, grants, or other support were received.

Competing interests: The author declares no competing interests.

Author contributions: Single-author work: conceptualization, derivation, implementation, experiments, writing.

Software: Orekit APIs and implementations were used for baseline comparison and truth generation setup [8].

A Expanded Scalar Derivation in One Block

Starting from Eq. (24)–(25), write

$$y_1 = -(b_1 + \rho_m e_1), \tag{37}$$
$$y_2 = -(b_2 + \rho_m e_2), \tag{38}$$
$$\Delta = 2(d_1 g_2 - d_2 g_1). \tag{39}$$

Then

$$u_{\tan}(\rho_m) = \frac{2d_1 y_2 - 2d_2 y_1}{\Delta} = \frac{2(-d_1 b_2 + d_2 b_1) + 2\rho_m(-d_1 e_2 + d_2 e_1)}{\Delta}. \tag{40}$$

Also

$$u_{\text{geom}}(\rho_m) = \mu \left(\|\mathbf{R}_m + \rho_m \hat{\boldsymbol{\ell}}_m\|^2 \right)^{-3/2}. \tag{41}$$

So

$$F(\rho_m) = \frac{2(-d_1 b_2 + d_2 b_1) + 2\rho_m(-d_1 e_2 + d_2 e_1)}{\Delta} - \mu \left(\|\mathbf{R}_m + \rho_m \hat{\boldsymbol{\ell}}_m\|^2 \right)^{-3/2}. \tag{42}$$

This explicit form is exactly what is sampled and bracketed numerically.

B Diagnostics Used in Code

Beyond residual metrics, TTC-3 records:

- $|F(\rho_m)|$ at selected solution,
- tangent 2×2 condition number,
- two-body energy relative drift,
- angular momentum relative drift,
- acceleration model mismatch RMS.

These diagnostics are intended to make failure cases inspectable rather than hidden.

References

[1] R. H. Gooding. A new procedure for the solution of the classical problem of minimal orbit determination from three lines of sight. *Celestial Mechanics and Dynamical Astronomy*, 66(4): 387–423, 1997. doi: 10.1007/BF00049379.

[2] A. J. Sarnecki. A projective approach to orbit determination from three sight-lines. *Celestial Mechanics and Dynamical Astronomy*, 66(4):425–451, 1997. doi: 10.1007/BF00049380.

[3] David A. Vallado. *Fundamentals of Astrodynamics and Applications*. Microcosm Press and Springer, 4 edition, 2013.

[4] Roger R. Bate, Donald D. Mueller, and Jerry E. White. *Fundamentals of Astrodynamics*. Dover Publications, 1971.

[5] G. F. Gronchi, G. Baù, and S. Marò. Orbit determination with the two-body integrals: Iii. *Celestial Mechanics and Dynamical Astronomy*, 123(2):105–122, 2015. doi: 10.1007/s10569-015-9623-6.

[6] Erica Scantamburlo, Giovanni F. Gronchi, and Giulio Baù. Orbit determination from one position vector and a very short arc of optical observations. *Celestial Mechanics and Dynamical Astronomy*, 136(4), 2024. doi: 10.1007/s10569-024-10201-7.

[7] Michela Mancini, Timothy Duff, Anton Leykin, and John A. Christian. Geometric solution to the angles-only initial orbit determination problem. *The Journal of the Astronautical Sciences*, 72(5), 2025. doi: 10.1007/s40295-025-00529-z.

[8] Orekit Development Team. Orekit initial orbit determination api. https://www.orekit.org/site-orekit-development/apidocs/org/orekit/estimation/iod/package-summary.html, 2026. Accessed 2026-02-17.